Optical Engineering 46(9), 094002 (September 2007)

Optimal design of retroreflection corner-cube sheets by geometric optics analysis

Hwi Kim
Byoungho Lee, FELLOW SPIE
Seoul National University
School of Electrical Engineering
Kwanak-Gu Shinlim-Dong
Seoul 151-744, Korea
E-mail: byoungho@snu.ac.kr

Abstract. We describe the geometric optic design and analysis of the optimal retroreflection corner-cube sheets with the effective retroreflective area ratio of 100%. The maximum condition of the effective retroreflective area of elementary retroreflection corner-cube is investigated, and as a result, the analytic design formulas of optimal retroreflection corner-cube structure are derived. We propose a novel packing method for the elementary retroreflection corner-cube to construct optimal retroreflection corner-cube sheets with the effective retroreflective area ratio of 100%. © *2007 Society of Photo-Optical Instrumentation Engineers.*
[DOI: 10.1117/1.2779030]

Subject terms: retroreflection corner-cube; geometric optics analysis; effective retroreflective area.

Paper 060830R received Oct. 24, 2006; revised manuscript received Mar. 10, 2007; accepted for publication Apr. 10, 2007; published online Sep. 10, 2007.

1 Introduction

Optical reflection for engineering applications can be classified into three types, as shown in Fig. 1: specular reflection, diffusing reflection, and retroreflection. The specular reflection is a simple reflection that occurs when an optical ray bundle is incident on a mirror, as shown in Fig. 1(a). Figure 1(b) shows the diffusing reflection, which is the complex backscattering of an incident optical ray bundle by a reflection surface having coarse surface roughness or internal volume scatters. This diffusing reflection is the basic property of general projection display screens; high-performance diffusing reflection is particularly important in the backlight systems of liquid crystal displays (LCDs). The retroreflection is a special reflection of ray bundle that returns back to the source origin along the inverse direction of the incident optical ray bundle, as indicated in Fig. 1(c).

For realizing the retroreflection, a specifically designed optical device called a retroreflector is needed. Several types of retroreflectors and their optical properties have been intensively investigated.[1–6] The most well-known retroreflector is the retroreflection corner-cube, which is schematically described in Fig. 2. They are used in many practical applications, such as positioning and guidance systems,[7–9] wavefront correction,[10] optical communications,[11] and traffic control signs.[12–14] In particular, retroreflectors are considered the key element of a new application, head-mounted projective displays, which incorporate great technology advancements that have been made in recent years.[15–21]

Several design criteria of retroreflection corner-cubes include retroreflectance, brightness, angularity, and divergence. But there are tradeoffs among these criteria, and the most important feature depends on each application. For example, in traffic applications, the intentional slight mismatch or flaws of retroreflection direction to incidence direction and a wide angularity of retroreflected light[14] are desirable. However, the most fundamental design issue of the retroreflection corner-cube for most applications is the maximization of the effective retroreflective area. The effective retroreflective area is the practical area on the incidence facet through which the incident ray bundle passes and is properly retroreflected.[2] The effective retroreflective area of a retroreflection corner-cube is varied for the incidence direction of the optical ray bundle. An optimal structure for the retroreflection corner-cube that has the maximum effective retroreflective area exists for a specific incidence direction. In practical applications, a sheet form to join many identical retroreflection corner-cubes is often fabricated. An optimal sheet structure having maximum effective retroreflective area also exists.

This paper describes a geometric optics analysis for the optimal design of retroreflection corner-cube sheets. A mathematical theorem about the optimal structure of a single retroreflection corner-cube with maximum effective retroreflective area is proposed, and from this theorem a few analytic design formulas of optimal retroreflection corner-cubes are derived. Based on this geometric optics analysis, a novel packing method of elementary retroreflection corner-cubes for constructing the optimal retroreflection corner-cube sheet having a 100% effective retroreflective area is proposed.

This paper is organized as follows. In Sec. 2, a geometric optics analysis on the effective retroreflective area of a single retroreflection corner-cube is presented, and the mathematical theorem about the optimal retroreflection corner-cube structure is proved. Section 3 describes the proposed packing method of elementary retroreflection corner-cubes with a related geometric optics analysis. Section 4 contains concluding remarks.

2 Geometric Optics Analysis on the Effective Retroreflective Area of a Single Retroreflection Corner-Cube

In general, a retroreflection corner-cube has the form of a trigonal pyramid composed of four facets, as shown in Fig.

0091-3286/2007/$25.00 © 2007 SPIE

Downloaded From: https://www.spiedigitallibrary.org/journals/Optical-Engineering on 10 Feb 2022
Terms of Use: https://www.spiedigitallibrary.org/terms-of-use

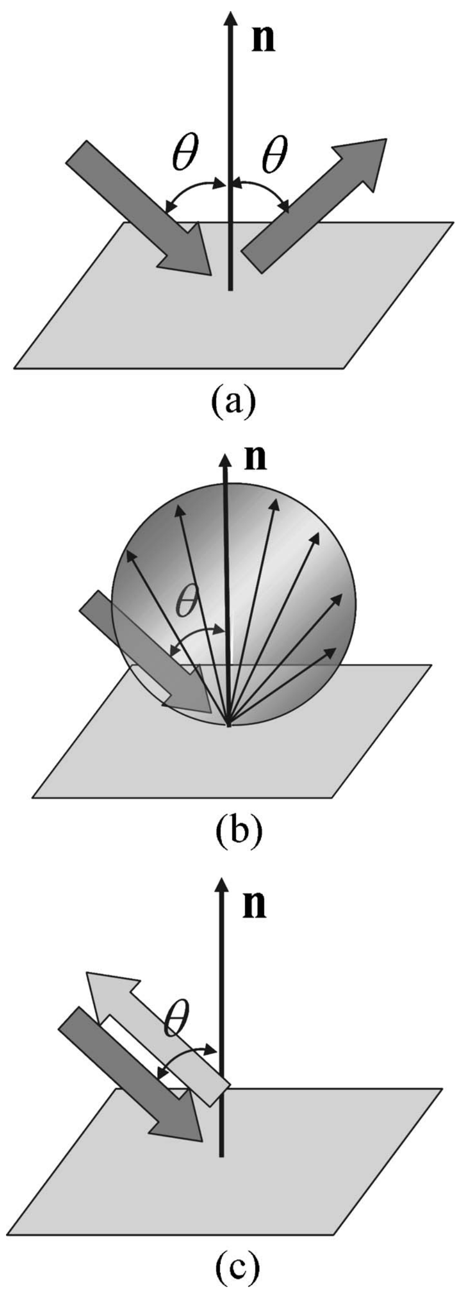

Fig. 1 (a) Specular reflection. (b) Diffusing reflection. (c) Retroreflection.

2. The ceiling facet is the incidence facet through which rays enter into the structure. Three other facets reflect incident rays. For the complete retroreflection, three dihedral angles between adjacent reflection facets must be exactly 90 deg. There are basically two-types of retroreflection corner-cubes: the total internal reflection (TIR) corner-cube, and the metal-coated mirror reflection corner-cube.

The TIR corner-cube is based on the TIR on the facets. In this case, the facet is uncoated and the TIR condition must be simultaneously satisfied on three facets so that a complete retroreflection occurs. In the metal-coated mirror reflection corner-cube, three reflection facets are metal-coated and the retroreflection occurs by three specular reflections on three metal-coated facets. In general, the TIR

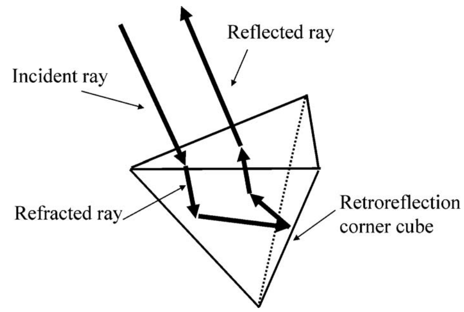

Fig. 2 Retroreflection corner-cube.

corner-cube is considered to be more advantageous than the metal-coated corner cube because the TIR corner-cube is cheaper, more efficient, structurally simple, and easier to fabricate than the metal-coated corner-cube.

In this section, a geometric optics analysis on the effective retroreflective area of a single retroreflection corner-cube is described. For convenience, the term "corner-cube" will be used to indicate a general retroreflection corner-cube. The analysis presented in this paper is so general that it is equally pertinent to TIR corner-cubes and metal-coated mirror reflection corner-cubes. Through this analysis, we can prove a mathematical theorem and derive a few useful formulas about the optimal corner-cube structure.

Assuming the dihedral angles between adjacent reflection facets are exactly 90 deg, we can set the schematic of a single corner-cube for the convenience of geometric analysis as shown in Fig. 3(a). Let the coordinate system adopted here be considered as the local coordinate system of the corner-cube. The corner-cube structure depicted on its local coordinate system is completely parameterized by three positive real numbers, x_0, y_0, and z_0, as shown in Fig. 3(a).

In the local coordinate system, the plane equation of the incidence facet of the corner-cube is given by

$$\frac{x}{x_0}+\frac{y}{y_0}+\frac{z}{z_0}=1, \tag{1a}$$

where x, y, and z are in the regions of $0\leqslant x$, $0\leqslant y$, and $0\leqslant z$, respectively. For convenience, x_0, y_0, and z_0 are normalized as

$$\left(\frac{1}{x_0}\right)^2+\left(\frac{1}{y_0}\right)^2+\left(\frac{1}{z_0}\right)^2=1. \tag{1b}$$

In Fig. 3(a), two parallel rays, l_1 and l_2, are incident on the incidence facet of the corner-cube, where l_1 is completely retroreflected but l_2 is not. For a clear comparison, the reflected rays of l_1 and l_2 are denoted by $\bar{l}_1$ and $\bar{l}_2$, respectively. An intuitive geometric analysis using mirror symmetry can be employed to analyze the respective internal ray traces of two rays. For easy understanding of this method, a 2-D analogy of this ray-tracing analysis using mirror symmetry is depicted in Fig. 3(b), where a ray enters into the structure as it passes point A, then the incident ray is refracted into the structure. The ray is reflected at point B and continues to strike the point $\bar{C}$. This ray trace can be

Downloaded From: https://www.spiedigitallibrary.org/journals/Optical-Engineering on 10 Feb 2022
Terms of Use: https://www.spiedigitallibrary.org/terms-of-use

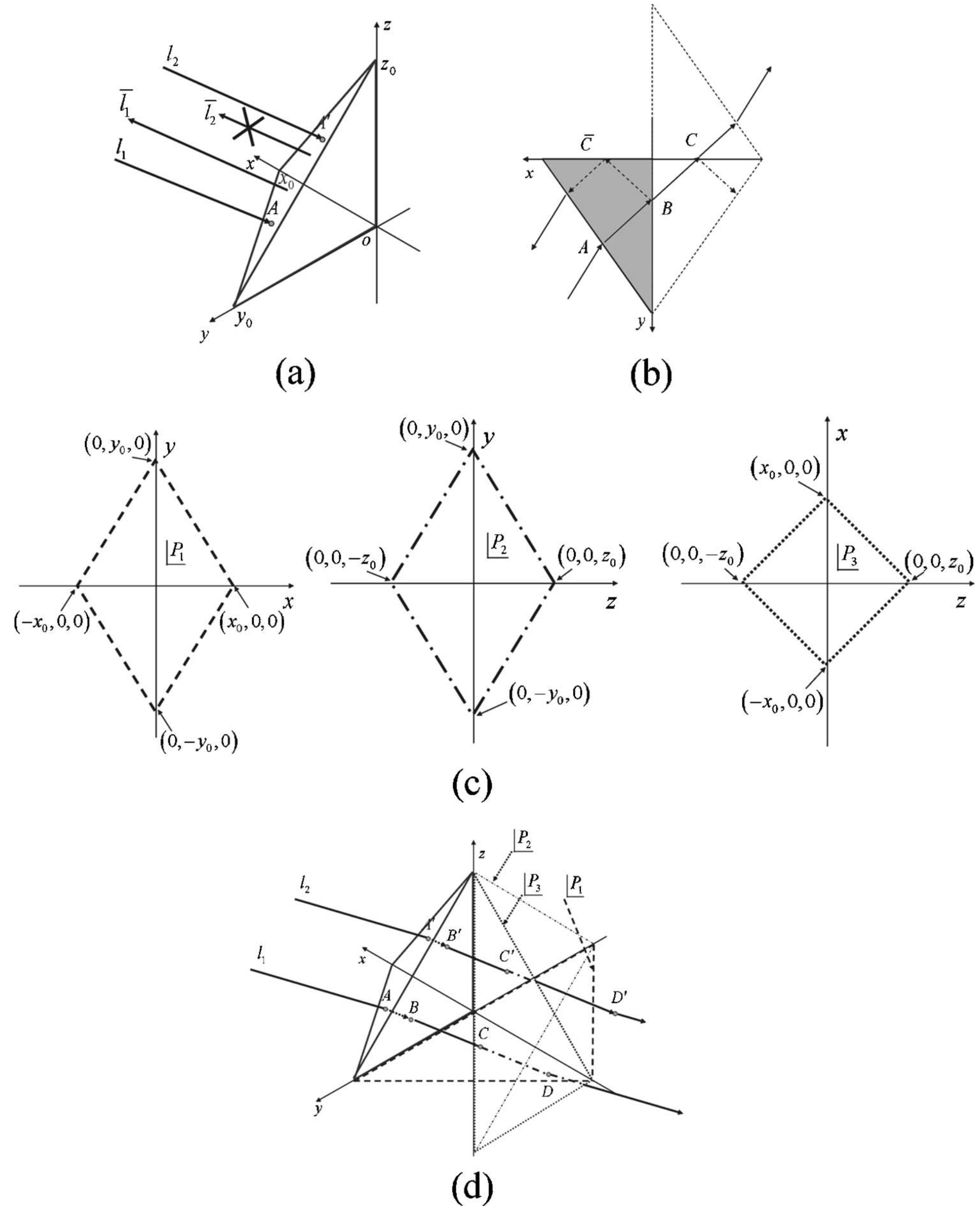

Fig. 3 (a) A single corner-cube depicted on its local coordinate system. (b) Two-dimensional analogy of the geometric ray-tracing analysis using mirror symmetry. (c) Definition of the retroreflection region P_1, P_2, and P_3. (d) Three-dimensional ray-tracing analysis of a single corner-cube using mirror symmetry.

equivalently described by the straight path connecting points A, B, and C. Point C corresponds to the mirror-symmetric point $\bar{C}$. This kind of geometric analysis using mirror symmetry may be useful for analyzing several specific optical geometries.[22]

We can apply this geometric analysis method using mirror symmetry to the analysis of corner-cubes. At first, the lozenge regions, P_1, P_2, and P_3, are defined in the x-y, y-z, and z-x planes, respectively, as shown in Fig. 3(c). These regions together are called the "retroreflection region." The direction vector of the ray entering into the structure, denoted by (k_x, k_y, k_z), is that of the ray in the medium of the corner-cube that already experienced the refraction on the boundary of the corner-cube's incidence facet and the surround (i.e., air). When a ray with the direction vector (k_x, k_y, k_z) passes the retroreflection regions P_1, P_2, and P_3, the direction vector components of the corresponding reflected ray, k_z, k_x, k_y, are changed to $-k_z$, $-k_x$, and $-k_y$, respectively. Therefore, when the ray passes through P_1, P_2, and P_3 successfully without an exception, the final reflected ray has the direction vector of the retroreflection, $(-k_x, -k_y, -k_z)$. Figure 3(d) shows the respective ray traces of rays l_1 and l_2 with direction vectors $(k_{1,x}, k_{1,y}, k_{1,z})$ and $(k_{2,x}, k_{2,y}, k_{2,z})$, respectively. Ray l_1 passing by point A meets point B in the region P_2, the point C in the region P_1, and finally, point D in the region P_3, successively. Since all cross points B, C, and D are inside the retroreflection re-

Downloaded From: https://www.spiedigitallibrary.org/journals/Optical-Engineering on 10 Feb 2022
Terms of Use: https://www.spiedigitallibrary.org/terms-of-use

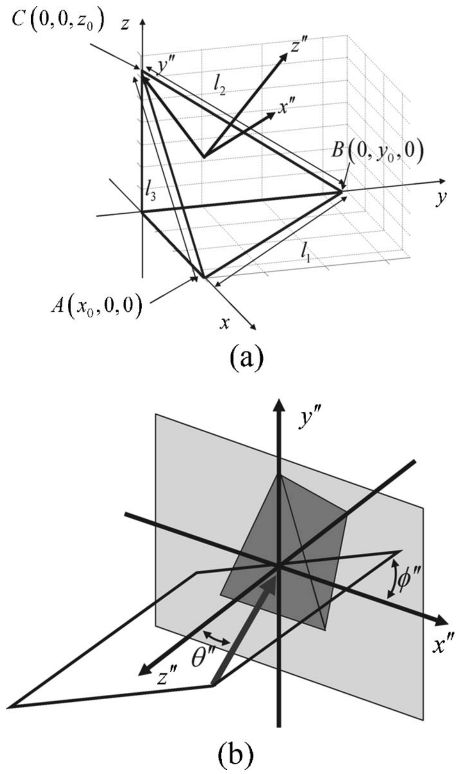

Fig. 4 (a) Relationship between the local coordinate system and the global coordinate system. (b) An incident optical ray bundle with the incidence angle θ'' and the azimuth angle ϕ'' in the global coordinate system.

gion, the ray l_1 is definitely retroreflected, so the reflected ray $\overline{l}_1$ has the direction vector of $(-k_{1,x},-k_{1,y},-k_{1,z})$. On the other hand, ray l_2 passing by point A' meets point B' in the region P_2, point C' in the region P_3, and point D', successively. Point D' is outside the region P_1. As a result, ray l_2 is not retroreflected. Since ray l_2 passes through just regions P_2 and P_3, the reflected ray $\overline{l}_2$ has the direction vector $(-k_{2,x},-k_{2,y},k_{2,z})$.

We can analyze the effective retroreflective area of the corner-cube within the framework of Fig. 3(d). Before doing this task, let us define the global coordinate system (x'',y'',z''). In the global coordinate system, the incidence facet of the corner-cube is placed on the x''-y'' plane and the z'' axis is set to direct the opposite direction of the apex point of the corner-cube. Figure 4(a) shows the global coordinate system within the framework of the local coordinate system, where point C of the incidence facet is set to be on the positive part of the y'' axis. Then we can establish the relationship between this local coordinate system (x,y,z) and the global coordinate system (x'',y'',z'') shown in Fig. 4(b). In the local coordinate system, the normal vector $\mathbf{n}$ to the incidence facet of the corner-cube is parameterized by θ_s and ϕ_s as

$$\mathbf{n}=(1/x_0,1/y_0,1/z_0)=(\cos\phi_s\sin\theta_s,\sin\phi_s\sin\theta_s,\cos\theta_s). \tag{2}$$

In Eq. (2), $\cos\theta_s$, $\sin\theta_s$, $\cos\phi_s$, and $\sin\phi_s$ can be solved for x_0, y_0, and z_0. In the configuration shown in Fig. 4(a), a spatial point (x,y,z) in the local coordinate system is represented by a point (x'',y'',z'') in the global coordinate system as

$$\begin{bmatrix} x-x_m \\ y-y_m \\ z-z_m \end{bmatrix}=\begin{bmatrix} \cos\phi_s\cos\theta_s & -\sin\phi_s & \cos\phi_s\sin\theta_s \\ \sin\phi_s\cos\theta_s & \cos\phi_s & \sin\phi_s\sin\theta_s \\ -\sin\theta_s & 0 & \cos\theta_s \end{bmatrix} \times\begin{bmatrix} 0 & -1 & 0 \\ 1 & 0 & 0 \\ 0 & 0 & 1 \end{bmatrix}\begin{bmatrix} x'' \\ y'' \\ z'' \end{bmatrix}, \tag{3}$$

where (x_m,y_m,z_m) is the crossing point of the normal vector $\mathbf{n}$ of Eq. (2) passing through the origin of the coordinate system and the incidence facet of the corner-cube of Eq. (1a), which is given by

$$(x_m,y_m,z_m)=(1/x_0,1/y_0,1/z_0) \tag{4}$$

and corresponds to the origin of the global coordinate system. In addition, a vector representation (k_x,k_y,k_z) in the local coordinate system is connected to the vector representation (k''_x,k''_y,k''_z) in the global coordinate system through the relation

$$\begin{bmatrix} k_x \\ k_y \\ k_z \end{bmatrix}=\begin{bmatrix} \cos\phi_s\cos\theta_s & -\sin\phi_s & \cos\phi_s\sin\theta_s \\ \sin\phi_s\cos\theta_s & \cos\phi_s & \sin\phi_s\sin\theta_s \\ -\sin\theta_s & 0 & \cos\theta_s \end{bmatrix} \times\begin{bmatrix} 0 & -1 & 0 \\ 1 & 0 & 0 \\ 0 & 0 & 1 \end{bmatrix}\begin{bmatrix} k''_x \\ k''_y \\ k''_z \end{bmatrix}. \tag{5}$$

Figure 4(b) shows that an optical ray bundle with the incidence angle of θ'' and the azimuth angle of ϕ'' is incident on the incidence facet of a corner-cube. The direction vector $(k''_{i,x},k''_{i,y},k''_{i,z})$ of the incident optical ray bundle is represented by

$$(k''_{i,x},k''_{i,y},k''_{i,z})=(\cos\phi''\sin\theta'',\sin\phi''\sin\theta'',-\cos\theta''). \tag{6}$$

This incident ray bundle goes to and is refracted into the corner-cube. The direction vector of the refracted ray bundle (k''_x,k''_y,k''_z) in a material with refractive index n is obtained by Snell's law:

$$\begin{aligned}(k''_x,k''_y,k''_z)&=\frac{1}{n}[\cos\phi''\sin\theta'',\sin\phi''\sin\theta'',-\sqrt{n^2-(\sin\theta'')^2}]\\ &=(\cos\phi\sin\theta,\sin\phi\sin\theta,-\cos\theta),\end{aligned} \tag{7}$$

where θ and ϕ are the refraction incidence angle and the refraction azimuth angle, respectively. This direction vector of the refracted ray is represented as (k_x,k_y,k_z) in the local coordinate system through the relation of Eq. (5).

As previously mentioned, corner-cubes can be classified into TIR corner-cubes and metal-coated mirror reflection corner-cubes. We can see that in the case of the TIR corner-cube, to achieve the proper TIRs at the retroreflection regions P_1, P_2, and P_3, the angles between the incident ray and the normal vectors of the x-$y(P_1)$, y-$z(P_2)$, and z-$x(P_3)$

Downloaded From: https://www.spiedigitallibrary.org/journals/Optical-Engineering on 10 Feb 2022
Terms of Use: https://www.spiedigitallibrary.org/terms-of-use

planes must be larger than the TIR critical angle of the corner-cube material. These conditions are represented as

$$|k_x| \leqslant \cos\theta_c, \tag{8a}$$

$$|k_y| \leqslant \cos\theta_c, \quad \text{and} \tag{8b}$$

$$|k_z| \leqslant \cos\theta_c, \tag{8c}$$

where θ_c is the TIR critical angle of the corner-cube material. In the case of the metal-coated mirror reflection corner-cube, any ray with an arbitrary direction incident on the metal-coated facet is specular-reflected unconditionally. Hence, in this case, it can be stated that the critical angle θ_c is zero. Therefore, Eqs. (8a)–(8c) are valid for both the metal-coated mirror reflection corner-cube and the TIR corner-cube.

Within this framework, we can proceed to the analysis on the effective retroreflective areas of both types of corner-cubes. An incident refracted ray with the direction vector (k_x, k_y, k_z) originated from an incidence point $(\bar{x}, \bar{y}, \bar{z})$ on the incident facet meets three cross points at three orthogonal x-y, y-z, and z-x planes, which are given, respectively, as:

$$(x_{xy}, y_{xy}, z_{xy}) = \left(-\frac{k_x\bar{z}}{k_z} + \bar{x}, -\frac{k_y\bar{z}}{k_z} + \bar{y}, 0\right), \quad \text{in the } x-y \text{ plane}, \tag{9a}$$

$$(x_{yz}, y_{yz}, z_{yz}) = \left(0, -\frac{k_y\bar{x}}{k_x} + \bar{y}, -\frac{k_z\bar{x}}{k_x} + \bar{z}\right), \quad \text{in the } y-z \text{ plane, and} \tag{9b}$$

$$(x_{zx}, y_{zx}, z_{zx}) = \left(-\frac{k_x\bar{y}}{k_y} + \bar{x}, 0, -\frac{k_z\bar{y}}{k_y} + \bar{z}\right), \quad \text{in the } z-x \text{ plane}. \tag{9c}$$

The necessary condition for the proper retroreflection is that three points of Eqs. (9a)–(9c) must be inside the retroreflection regions P_1, P_2, and P_3, respectively, which is represented by the following inequalities:

$$-1 < -\frac{x_{xy}}{x_0} + \frac{y_{xy}}{y_0} < 1, \tag{10a}$$

$$-1 < \frac{x_{xy}}{x_0} + \frac{y_{xy}}{y_0} < 1, \tag{10b}$$

$$-1 < -\frac{z_{yz}}{z_0} + \frac{y_{yz}}{y_0} < 1, \tag{11a}$$

$$-1 < \frac{z_{yz}}{z_0} + \frac{y_{yz}}{y_0} < 1, \tag{11b}$$

$$-1 < -\frac{z_{zx}}{z_0} + \frac{x_{zx}}{x_0} < 1, \quad \text{and} \tag{12a}$$

$$-1 < \frac{z_{zx}}{z_0} + \frac{x_{zx}}{x_0} < 1. \tag{12b}$$

By substituting Eqs. (9a)–(9c) into Eqs. (10a), (10b), (11a), (11b), (12a), and (12b), we can obtain a set of six inequalities with respect to $(\bar{x}, \bar{y})$ as

$$\begin{aligned}\frac{(k_x/x_0)}{(k_z/z_0)} + \frac{(k_y/y_0)}{(k_z/z_0)} - 1 &< \left\{\left[\frac{(k_x/x_0)}{(k_z/z_0)} + 1\right] + \frac{(k_y/y_0)}{(k_z/z_0)}\right\}(\bar{x}/x_0) \\ &\quad + \left\{\left[\frac{(k_y/y_0)}{(k_z/z_0)} + 1\right] + \frac{(k_x/x_0)}{(k_z/z_0)}\right\}(\bar{y}/y_0) \\ &< 1 + \frac{(k_x/x_0)}{(k_z/z_0)} + \frac{(k_y/y_0)}{(k_z/z_0)},\end{aligned} \tag{13a}$$

$$\begin{aligned}-\frac{(k_x/x_0)}{(k_z/z_0)} + \frac{(k_y/y_0)}{(k_z/z_0)} - 1 &< \left\{-\left[\frac{(k_x/x_0)}{(k_z/z_0)} + 1\right] + \frac{(k_y/y_0)}{(k_z/z_0)}\right\} \\ &\quad \times (\bar{x}/x_0) + \left\{\left[\frac{(k_y/y_0)}{(k_z/z_0)} + 1\right]\right. \\ &\quad \left. - \frac{(k_x/x_0)}{(k_z/z_0)}\right\}(\bar{y}/y_0) < 1 - \frac{(k_x/x_0)}{(k_z/z_0)} \\ &\quad + \frac{(k_y/y_0)}{(k_z/z_0)},\end{aligned} \tag{13b}$$

$$0 < \left[\frac{(k_z/z_0)}{(k_x/x_0)} + \frac{(k_y/y_0)}{(k_x/x_0)} + 1\right](\bar{x}/x_0) < 2, \tag{13c}$$

$$0 < \left[\frac{(k_z/z_0)}{(k_y/y_0)} + \frac{(k_x/x_0)}{(k_y/y_0)} + 1\right](\bar{y}/y_0) < 2, \tag{13d}$$

$$0 < \left[\frac{(k_z/z_0)}{(k_x/x_0)} + 1 - \frac{(k_y/y_0)}{(k_x/x_0)}\right](\bar{x}/x_0) + 2(\bar{y}/y_0) < 2, \quad \text{and} \tag{13e}$$

$$0 < \left[\frac{(k_z/z_0)}{(k_y/y_0)} + 1 - \frac{(k_x/x_0)}{(k_y/y_0)}\right](\bar{y}/y_0) + 2(\bar{x}/x_0) < 2. \tag{13f}$$

Here the main task is to find the condition that maximizes the area of $(\bar{x}, \bar{y})$ and satisfies Eqs. (13a)–(13f).

The first case to be investigated is that of the symmetric TIR corner-cube. The refractive indices of the corner-cube material and the surround are set to 1.55 and 1, respectively. Figure 5 displays the effective retroreflective areas of the symmetric corner-cube ($x_0 = \sqrt{3}$, $y_0 = \sqrt{3}$, $z_0 = \sqrt{3}$) for several incidence directions. The calculated effective retroreflective areas are the images projected onto the incidence facet of the corner-cube in the areas of $(\bar{x}, \bar{y})$ that satisfy Eqs. (13a)–(13f). Let the effective retroreflective area ratio η be defined by the ratio (%) of the effective retroreflective area to the total area of the incidence facet of

Downloaded From: https://www.spiedigitallibrary.org/journals/Optical-Engineering on 10 Feb 2022
Terms of Use: https://www.spiedigitallibrary.org/terms-of-use

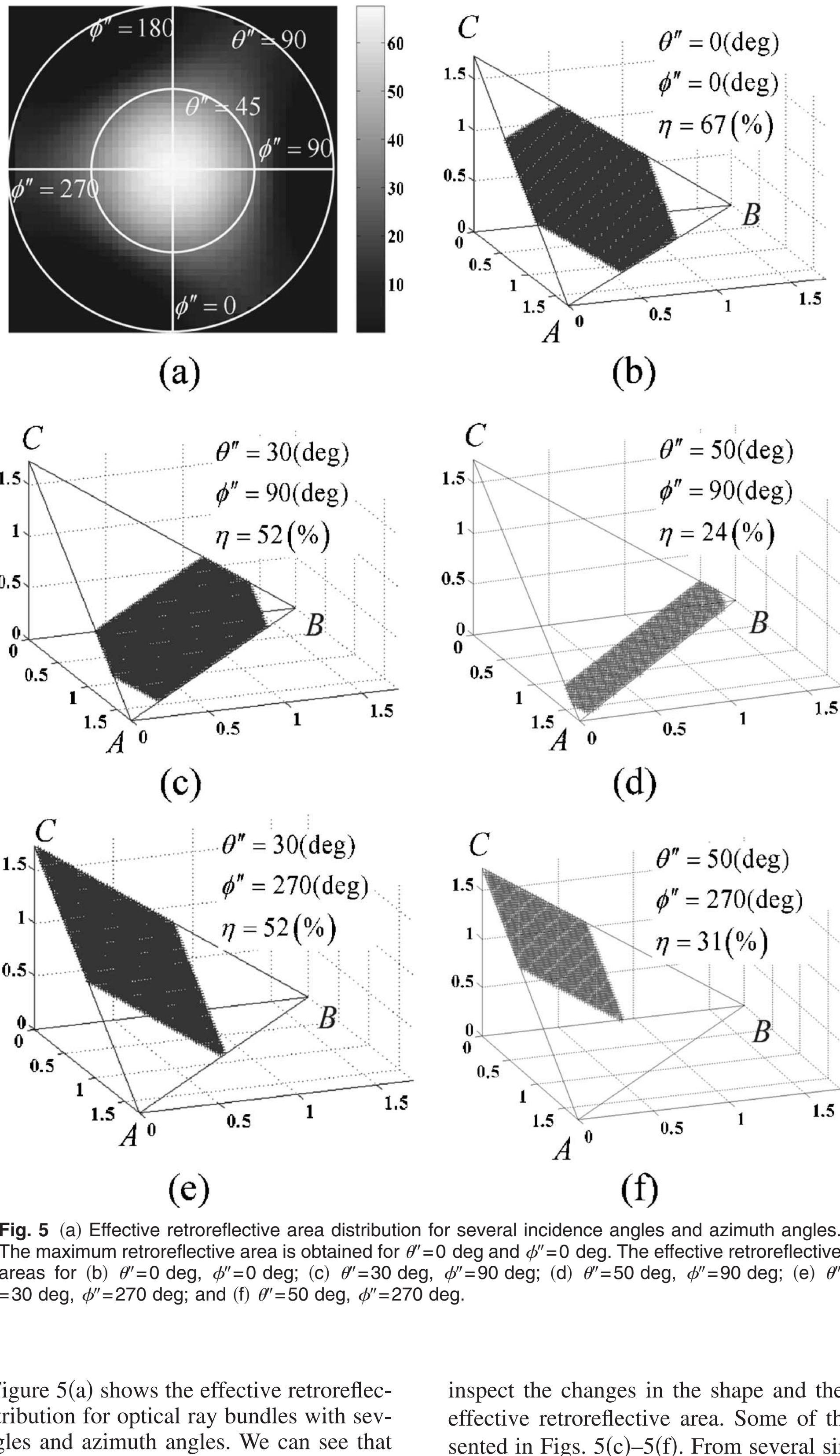

Fig. 5 (a) Effective retroreflective area distribution for several incidence angles and azimuth angles. The maximum retroreflective area is obtained for $\theta''=0$ deg and $\phi''=0$ deg. The effective retroreflective areas for (b) $\theta''=0$ deg, $\phi''=0$ deg; (c) $\theta''=30$ deg, $\phi''=90$ deg; (d) $\theta''=50$ deg, $\phi''=90$ deg; (e) $\theta''=30$ deg, $\phi''=270$ deg; and (f) $\theta''=50$ deg, $\phi''=270$ deg.

the corner-cube. Figure 5(a) shows the effective retroreflective area ratio distribution for optical ray bundles with several incidence angles and azimuth angles. We can see that for this corner-cube, the maximum effective retroreflective area ratio of 67% is obtained for the incident optical ray bundle with the normal incidence angle of $\theta=0$ deg. As shown in Fig. 5(b), the shape of the maximum effective retroreflective area is a hexagon. We can vary the incidence angles and the azimuth angles of the incident ray bundle to inspect the changes in the shape and the area ratio of the effective retroreflective area. Some of the results are presented in Figs. 5(c)–5(f). From several simulations, we can determine that the shapes of the effective retroreflective areas are classified into just lozenge and hexagon.

Based on the simulation result of the symmetric corner-cube ($x_0=\sqrt{3}$, $y_0=\sqrt{3}$, $z_0=\sqrt{3}$), we can derive the more general optimal condition of corner-cube structure. The follow-

Downloaded From: https://www.spiedigitallibrary.org/journals/Optical-Engineering on 10 Feb 2022
Terms of Use: https://www.spiedigitallibrary.org/terms-of-use

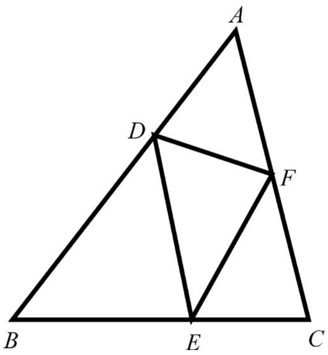

Fig. 6 Two triangles, ΔABC and ΔDEF.

ing theorem settles up this task.

Theorem: For an incident refracted ray bundle with the direction vector of $\mathbf{k}=(k_x,k_y,k_z)$ represented in the local coordinate system, the optimal corner-cube with maximum effective retroreflective area is that of $(x_0,y_0,z_0)/\sqrt{x_0^2+y_0^2+z_0^2}=(-k_x,-k_y,-k_z)$.

Proof: It has already been shown with the aid of numerical simulation that the optimal corner-cube structure for the optical ray bundle of $\mathbf{k}=(-1,-1,-1)/\sqrt{3}$ is that of the symmetric corner-cube $(x_0,y_0,z_0)=(\sqrt{3},\sqrt{3},\sqrt{3})$. Let us remind that the ratio of the areas of two arbitrary triangles ΔABC and ΔDEF is invariant even with a scaling coordinate transformation such as $(x,y,z)\rightarrow(ax,by,cz)$. Let's consider the two triangles ΔABC and ΔDEF shown in Fig. 6. The triangle ΔABC circumscribes the triangle ΔDEF. Without loss of generality, we can let the three apexes be denoted by $A=(x_1,y_1,z_1)$, $B=(x_2,y_2,z_2)$, and $C=(0,0,0)$. The dividing points, denoted by D, E, and F, are given, respectively, by

$$D=[\alpha x_1+(1-\alpha)x_2,\alpha y_1+(1-\alpha)y_2,\alpha z_1+(1-\alpha)z_2],\quad E=(\beta x_2,\beta y_2,\beta z_2),\quad \text{and } F=(\gamma x_1,\gamma y_1,\gamma z_1),$$

respectively. The areas of the triangles ΔABC and ΔDEF are given, respectively, by

$$S_{ABC}=\frac{1}{2}\sqrt{(x_2y_1-y_2x_1)^2+(y_2z_1-z_2y_1)^2+(x_2z_1-z_2x_1)^2}, \tag{14a}$$

and

$$S_{DEF}=\frac{[\beta(\alpha-\gamma)+\gamma(1-\alpha)]}{2}\sqrt{(x_2y_1-y_2x_1)^2+(y_2z_1-z_2y_1)^2+(x_2z_1-z_2x_1)^2}. \tag{14b}$$

From Eqs. (14a) and (14b), we can confirm that the ratio of S_{DEF} and S_{ABC} is invariant for the scaling coordinate transformation $(x,y,z)\rightarrow(ax,by,cz)$. Since general polygons are composed of elementary triangles, we can conclude that the ratio of the areas of two arbitrary polygons is invariant for the scaling coordinate transformation.

Now we are prepared to find the optimal corner-cube structure for an arbitrary incident optical ray bundle. Let k'_x, k'_y, k'_x, $\bar{x}'$, $\bar{y}'$, and $\bar{z}'$ be defined by $k'_x=k_x/x_0$, $k'_y=k_y/y_0$, $k'_z=k_z/z_0$, $\bar{x}'=\bar{x}/x_0$, $\bar{y}'=\bar{y}/y_0$, and $\bar{z}'=\bar{z}/z_0$, respectively. By substituting these variables into Eqs. (13a)–(13f), the following inequalities are obtained:

$$\frac{k'_x}{k'_z}+\frac{k'_y}{k'_z}-1<\left[\frac{k'_x}{k'_z}+\frac{k'_y}{k'_z}+1\right]\bar{x}'+\left[\frac{k'_x}{k'_z}+\frac{k'_y}{k'_z}+1\right]\bar{y}' <\frac{k'_x}{k'_z}+\frac{k'_y}{k'_z}+1, \tag{15a}$$

$$-\frac{k'_x}{k'_z}+\frac{k'_y}{k'_z}-1<\left[-\frac{k'_x}{k'_z}+\frac{k'_y}{k'_z}-1\right]\bar{x}'+\left[-\frac{k'_x}{k'_z}+\frac{k'_y}{k'_z}+1\right]\bar{y}' <-\frac{k'_x}{k'_z}+\frac{k'_y}{k'_z}+1, \tag{15b}$$

$$0<\left(1+\frac{k'_y}{k'_x}+\frac{k'_z}{k'_x}\right)\bar{x}'<2, \tag{15c}$$

$$0<\left(\frac{k'_x}{k'_y}+1+\frac{k'_z}{k'_y}\right)\bar{y}'<2, \tag{15d}$$

$$0<\left(1-\frac{k'_y}{k'_x}+\frac{k'_z}{k'_x}\right)\bar{x}'+2\bar{y}'<2, \quad \text{and} \tag{15e}$$

$$0<2\bar{x}'+\left(-\frac{k'_x}{k'_y}+1+\frac{k'_z}{k'_y}\right)\bar{y}'<2. \tag{15f}$$

Comparing Eqs. (15a)–(15f) and Eqs. (13a)–(13f), we can determine that Eqs. (15a)–(15f) have the same form as Eqs. (13a)–(13f) when (x_0,y_0,z_0) in Eqs. (13a)–(13f) is set to $(\sqrt{3},\sqrt{3},\sqrt{3})$. Therefore, the optimal value of (k'_x,k'_y,k'_z) to maximize the effective retroreflective area ratio is given by $(k'_x,k'_y,k'_z)=t(-1,-1,-1)$. This condition is equivalent to the relation

$$(-k_x,-k_y,-k_z)=t(x_0,y_0,z_0)\leftrightarrow(x_0,y_0,z_0)/\sqrt{x_0^2+y_0^2+z_0^2} =(-k_x,-k_y,-k_z). \tag{15g}$$

This concludes the proof of the theorem.

With the condition $(x_0,y_0,z_0)/\sqrt{x_0^2+y_0^2+z_0^2}=(-k_x,-k_y,-k_z)$ satisfied, the inequalities of Eqs. (15a)–(15f) read as

$$\frac{1}{3}<\bar{x}'+\bar{y}'<1\leftrightarrow\frac{1}{3}<\frac{\bar{x}}{x_0}+\frac{\bar{y}}{y_0}<1, \tag{16a}$$

$$-1<-\bar{x}'+\bar{y}'<1\leftrightarrow-1<-\frac{\bar{x}}{x_0}+\frac{\bar{y}}{y_0}<1, \tag{16b}$$

$$0<\bar{x}'<\frac{2}{3}\leftrightarrow 0<\frac{\bar{x}}{x_0}<\frac{2}{3}, \tag{16c}$$

Downloaded From: https://www.spiedigitallibrary.org/journals/Optical-Engineering on 10 Feb 2022
Terms of Use: https://www.spiedigitallibrary.org/terms-of-use

$$0 < \bar{y}' < \frac{2}{3} \leftrightarrow 0 < \frac{\bar{y}}{y_0} < \frac{2}{3}, \tag{16d}$$

$$0 < \bar{x}' + 2\bar{y}' < 2 \leftrightarrow 0 < \frac{\bar{x}}{x_0} + 2\frac{\bar{y}}{y_0} < 2, \quad \text{and} \tag{16e}$$

$$0 < 2\bar{x}' + \bar{y}' < 2 \leftrightarrow 0 < 2\frac{\bar{x}}{x_0} + \frac{\bar{y}}{y_0} < 2. \tag{16f}$$

The area constrained by the above inequalities is plotted in Fig. 7. In this case, the effective retroreflective area ratio is 67%.

By extending the theorem, we can obtain the following corollary about the corner-cube design formulas.

Corollary: When an optical ray bundle with the refraction incidence angle θ and the refraction azimuth angle ϕ is incident on the corner-cube in the global coordinate system, as shown in Fig. 4, we can build up the functional relationship between the optimal corner-cube structure (x_0, y_0, z_0) and the incidence direction parameter (θ, ϕ) of an optical ray bundle as follows:

$$x_0 = \frac{1}{\cos[\phi_s(\theta,\phi)]\sin[\theta_s(\theta,\phi)]}, \tag{17a}$$

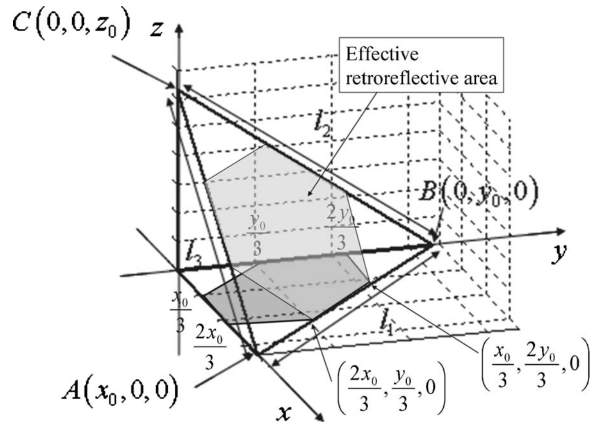

Fig. 7 Optimal corner-cube structure and its effective retroreflective area.

$$y_0 = \frac{1}{\sin[\phi_s(\theta,\phi)]\sin[\theta_s(\theta,\phi)]}, \quad \text{and} \tag{17b}$$

$$z_0 = \frac{1}{\cos[\theta_s(\theta,\phi)]}, \tag{17c}$$

where θ_s and ϕ_s are obtained with respect to θ and ϕ from the following relations:

$$\tan\theta_s = \frac{3\cos\left(\frac{\pi}{2}+\phi\right)\sin\theta + \sqrt{9\cos^2\left(\frac{\pi}{2}+\phi\right)\sin^2\theta + 8\cos^2\theta}}{2\cos\theta}, \tag{18a}$$

$$\tan\phi_s = \frac{\sin\left(\frac{\pi}{2}+\phi\right)\sin\theta\frac{\sin\theta_s}{t} + \sqrt{\left[\sin\left(\frac{\pi}{2}+\phi\right)\sin\theta\frac{\sin\theta_s}{t}\right]^2 + 4}}{2}, \tag{18b}$$

where t is given by
$$t = \cos\theta_s\sin\theta_s\cos\left(\frac{\pi}{2}+\phi\right)\sin\theta + \cos\theta_s\cos\theta_s\cos\theta. \tag{18c}$$

Proof: From the theorem, we know that the condition of the optimal corner-cube is given by

$$(k_x, k_y, k_z) = -t(x_0, y_0, z_0), \quad \text{where } t \text{ is give by } t = 1/\sqrt{x_0^2 + y_0^2 + z_0^2}. \tag{19}$$

The direction vector of the optical ray bundle with the refraction incidence angle θ and the refraction azimuth angle ϕ is given by Eq. (7). By substituting Eqs. (19) and (7) into Eq. (5) and using the relation of Eq. (2), we can obtain

$$t\begin{bmatrix} -\dfrac{1}{\cos\phi_s\sin\theta_s} \\ -\dfrac{1}{\sin\phi_s\sin\theta_s} \\ -\dfrac{1}{\cos\theta_s} \end{bmatrix} = \begin{bmatrix} \cos\phi_s & -\sin\phi_s & 0 \\ \sin\phi_s & \cos\phi_s & 0 \\ 0 & 0 & 1 \end{bmatrix} \times \begin{bmatrix} \cos\theta_s & 0 & \sin\theta_s \\ 0 & 1 & 0 \\ -\sin\theta_s & 0 & \cos\theta_s \end{bmatrix}\begin{bmatrix} 0 & -1 & 0 \\ 1 & 0 & 0 \\ 0 & 0 & 1 \end{bmatrix} \times \begin{bmatrix} \cos\phi\sin\theta \\ \sin\phi\sin\theta \\ -\cos\theta \end{bmatrix}. \tag{20}$$

Downloaded From: https://www.spiedigitallibrary.org/journals/Optical-Engineering on 10 Feb 2022
Terms of Use: https://www.spiedigitallibrary.org/terms-of-use

By further arrangement, Eq. (20) reads as

$$\begin{bmatrix} -2\dfrac{t}{\sin\theta_s} \\ \left(\tan\phi_s-\dfrac{1}{\tan\phi_s}\right)\dfrac{t}{\sin\theta_s} \\ -\dfrac{t}{\cos\theta_s} \end{bmatrix} = \begin{bmatrix} \cos\theta_s\cos\left(\dfrac{\pi}{2}+\phi\right)\sin\theta-\sin\theta_s\cos\theta \\ \sin\left(\dfrac{\pi}{2}+\phi\right)\sin\theta \\ -\sin\theta_s\cos\left(\dfrac{\pi}{2}+\phi\right)\sin\theta-\cos\theta_s\cos\theta \end{bmatrix}. \tag{21}$$

At this stage, we can find the solution to the above equations, θ_s and ϕ_s, as follows:

$$\tan\theta_s=\frac{3\cos\left(\dfrac{\pi}{2}+\phi\right)\sin\theta+\sqrt{9\cos^2\left(\dfrac{\pi}{2}+\phi\right)\sin^2\theta+8\cos^2\theta}}{2\cos\theta},\quad(\tan\theta_s>0) \tag{22a}$$

$$t=\cos\theta_s\sin\theta_s\cos\left(\frac{\pi}{2}+\phi\right)\sin\theta+\cos\theta_s\cos\theta_s\cos\theta, \tag{22b}$$

and

$$\tan\phi_s=\frac{\sin\left(\dfrac{\pi}{2}+\phi\right)\sin\theta\dfrac{\sin\theta_s}{t}+\sqrt{\left(\sin\left(\dfrac{\pi}{2}+\phi\right)\sin\theta\dfrac{\sin\theta_s}{t}\right)^2+4}}{2},\quad(\tan\phi_s>0). \tag{22c}$$

From Eq. (2), the optimal corner-cube structure for the incident optical ray bundle with the refraction incidence angle θ and the refraction azimuth angle ϕ is derived as

$$x_0=\frac{1}{\cos[\phi_s(\theta,\phi)]\sin[\theta_s(\theta,\phi)]}, \tag{23a}$$

$$y_0=\frac{1}{\sin[\phi_s(\theta,\phi)]\sin[\theta_s(\theta,\phi)]}, \tag{23b}$$

and

$$z_0=\frac{1}{\cos[\theta_s(\theta,\phi)]}. \tag{23c}$$

This concludes the proof of the corollary.

Using the corollary, we can obtain the design formulas about the lengths of edges l_1, l_2, and l_3 of the corner-cube, and the height h of the apex point, respectively, by

$$l_1=\sqrt{x_0^2+y_0^2}, \tag{24a}$$

$$l_2=\sqrt{y_0^2+z_0^2}, \tag{24b}$$

$$l_3=\sqrt{z_0^2+x_0^2},\quad\text{and} \tag{24c}$$

$$h=\frac{1}{\sqrt{\left(\dfrac{1}{x_0}\right)^2+\left(\dfrac{1}{y_0}\right)^2+\left(\dfrac{1}{z_0}\right)^2}}. \tag{24d}$$

In addition, we can extract the refraction incidence angle θ and the refraction azimuth angle ϕ of the optimal incident optical ray bundle to a given corner-cube structure by using the inversion of the corollary given by

$$\begin{bmatrix}\cos\phi\sin\theta\\ \sin\phi\sin\theta\\ -\cos\theta\end{bmatrix}=\frac{\begin{bmatrix}0&1&0\\-1&0&0\\0&0&1\end{bmatrix}\begin{bmatrix}\cos\theta_s\cos\phi_s&\cos\theta_s\sin\phi_s&-\sin\theta_s\\-\sin\phi_s&\cos\phi_s&0\\ \sin\theta_s\cos\phi_s&\sin\theta_s\sin\phi_s&\cos\theta_s\end{bmatrix}\begin{bmatrix}-\dfrac{1}{\cos\phi_s\sin\theta_s}\\-\dfrac{1}{\sin\phi_s\sin\theta_s}\\-\dfrac{1}{\cos\theta_s}\end{bmatrix}}{\sqrt{\left(\dfrac{1}{\cos\phi_s\sin\theta_s}\right)^2+\left(\dfrac{1}{\sin\phi_s\sin\theta_s}\right)^2+\left(\dfrac{1}{\cos\theta_s}\right)^2}}, \tag{24e}$$

Downloaded From: https://www.spiedigitallibrary.org/journals/Optical-Engineering on 10 Feb 2022
Terms of Use: https://www.spiedigitallibrary.org/terms-of-use

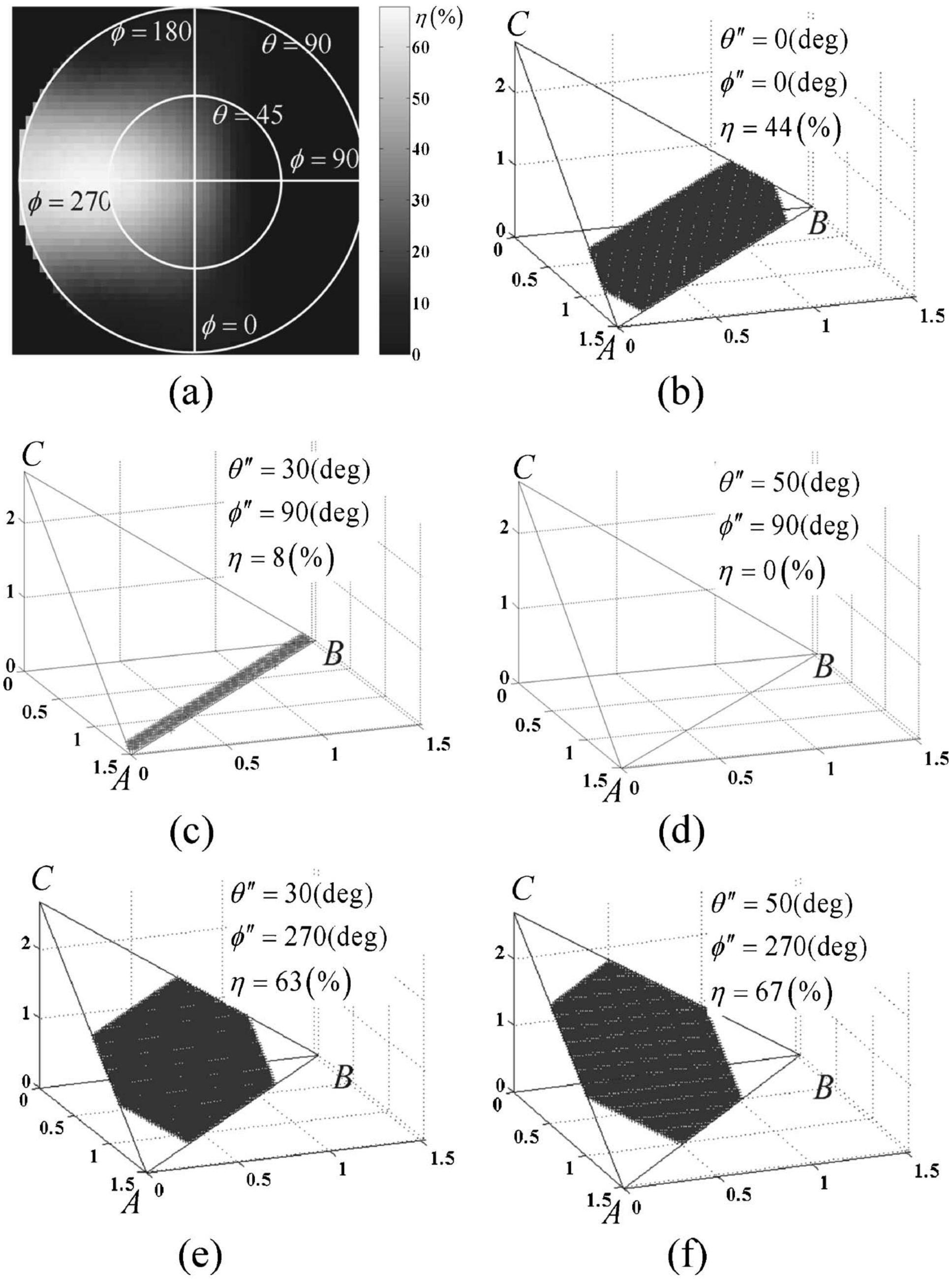

Fig. 8 (a) Effective retroreflective area distribution for several incidence angles and azimuth angles. The maximum retroreflective area is obtained for θ''=50 deg and ϕ''=270 deg. The effective retroreflective areas for (b) θ''=0 deg, ϕ''=0 deg; (c) θ''=30 deg, ϕ''=90 deg; (d) θ''=50 deg, ϕ''=90 deg; (e) θ''=30 deg, ϕ''=270 deg; and (f) θ''=50 deg, ϕ''=270 deg.

where θ_s and ϕ_s are the functions of the corner-cube parameters (x_0, y_0, z_0) defined by Eq. (8).

By substituting Eq. (24e) into Eq. (7), we can also find the incidence angle θ'' and the azimuth angle ϕ'' of the optimal incident optical ray bundle.

Next we will present an example to be compared to the results shown in Fig. 5. For the incidence angle θ'' =50 deg and the azimuth angle ϕ''=270 deg, the optimal structure parameters x_0, y_0, and z_0 of the corner-cube structure with the refractive index of 1.55 is obtained by x_0=1.5228, y_0=1.5228, and z_0=2.6965, respectively, which are calculated from Eq. (7) and Eqs. (17a)–(17c) and (18a)–(18c) of the corollary. Figure 8(a) shows the effective retroreflective area ratio distribution for optical ray bundles with several incidence angles and azimuth angles. As expected from the described theory, we can see that this corner-cube has the maximum effective retroreflective area ratio of 67% when the incidence angle θ and the azimuth angle ϕ of the incident optical ray bundle are θ=50 deg and ϕ=270 deg. The retroreflective areas obtained for sev-

Downloaded From: https://www.spiedigitallibrary.org/journals/Optical-Engineering on 10 Feb 2022
Terms of Use: https://www.spiedigitallibrary.org/terms-of-use

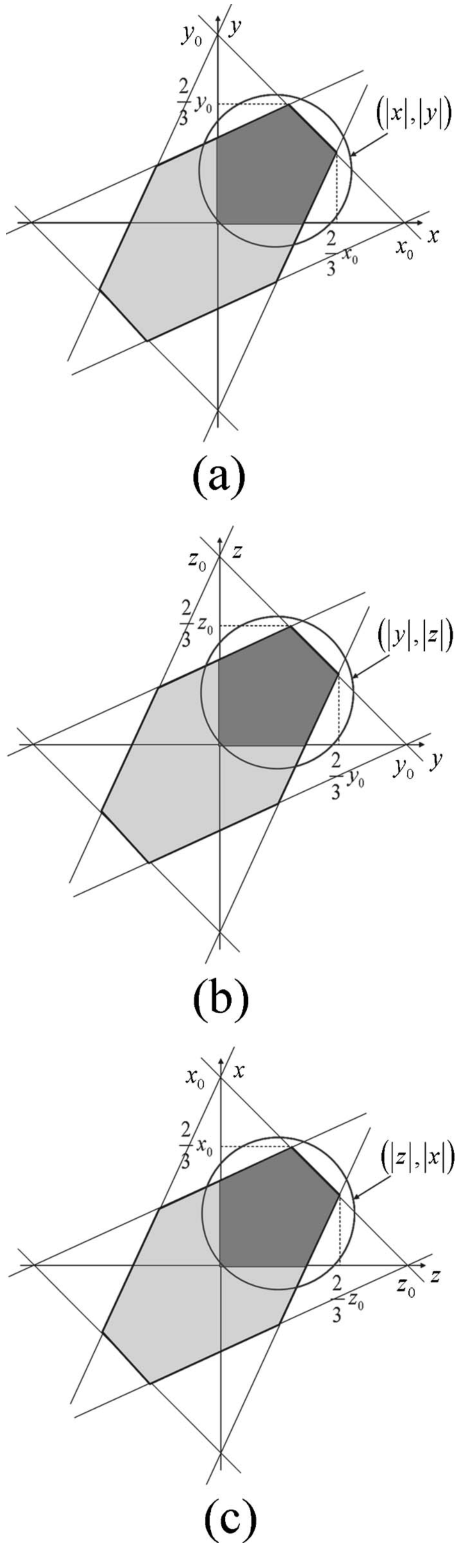

Fig. 9 Regions actually contributing the retroreflection in (a) the x-y plane, (b) the y-z plane, and (c) the z-x plane.

eral cases of the incidence angle and the azimuth angle are shown in Figs. 8(b)–8(f) for comparison with Figs. 5(b)–5(d) and 5(f). In the optimal case shown in Fig. 8(f), the shape of the retroreflective area is also a hexagon.

3 Optimal Packing Method of Retroreflection Corner-Cube Sheets

In practice, retroreflection corner-cubes are used in a sheet form with the periodic array of elementary corner-cubes.[2] In this section, based on the corollary derived in Sec. 2, a novel packing method of optimally designed elementary corner-cubes for constructing optimal corner-cube sheets is proposed. As analyzed in Sec. 2, the maximum effective retroreflective area ratio η of a single corner-cube is 67%. However, it can be shown that by constructing the sheet form of tightly and periodically arranged identical corner-cubes, we can obtain the maximum effective retroreflective area ratio of 100%. This optimization problem can be settled with an additional simple geometric analysis continued from Sec. 2.

Let us inspect the meaningful regions that actually contribute the retroreflection at the retroreflection regions, P_1, P_2, and P_3. From Eq. (1a), we know that

$$\bar{z}/z_0 = 1 - (\bar{x}/x_0 + \bar{y}/y_0). \tag{25}$$

By substituting Eq. (25) into Eqs. (9a)–(9c), the following relations hold:

$$(x_{xy}/x_0, y_{xy}/y_0, z_{xy}/z_0) = (-1 + 2\bar{x}/x_0 + \bar{y}/y_0, -1 + \bar{x}/x_0 + 2\bar{y}/y_0, 0) \quad \text{in the } x\text{-}y \text{ plane}, \tag{26a}$$

$$(x_{yz}/x_0, y_{yz}/y_0, z_{yz}/z_0) = (0, -\bar{x}/x_0 + \bar{y}/y_0, 1 - 2\bar{x}/x_0 - \bar{y}/y_0) \quad \text{in the } y\text{-}z \text{ plane}, \tag{26b}$$

and

$$(x_{zx}/x_0, y_{zx}/y_0, z_{zx}/z_0) = (-\bar{y}/y_0 + \bar{x}/x_0, 0, 1 - \bar{x}/x_0 - 2\bar{y}/y_0) \quad \text{in the } z\text{-}x \text{ plane}. \tag{26c}$$

By manipulating Eq. (26a) as

$$\begin{bmatrix} \bar{x}/x_0 \\ \bar{y}/y_0 \end{bmatrix} = \frac{1}{3}\begin{pmatrix} 2 & -1 \\ -1 & 2 \end{pmatrix}\begin{bmatrix} x_{xy}/x_0 + 1 \\ y_{xy}/y_0 + 1 \end{bmatrix} = \frac{1}{3}\begin{bmatrix} 2x_{xy}/x_0 - y_{xy}/y_0 + 1 \\ -x_{xy}/x_0 + 2y_{xy}/y_0 + 1 \end{bmatrix} \tag{27}$$

and substituting Eq. (27) into Eqs. (16a)–(16d) and (16f), we can obtain the inequalities that indicate the image of the effective retroreflective area projected onto the x-y plan:

$$-1 < x_{xy}/x_0 + y_{xy}/y_0 < 1, \tag{28a}$$

$$-1 < 2x_{xy}/x_0 - y_{xy}/y_0 < 1, \quad \text{and} \tag{28b}$$

$$-1 < 2y_{xy}/y_0 - x_{xy}/x_0 < 1. \tag{28c}$$

From the symmetry, we can also obtain the images of the effective retroreflective area projected onto the y-z plane and the z-x plane, respectively, as:

$$-1 < y_{yz}/y_0 + z_{yz}/z_0 < 1, \tag{29a}$$

$$-1 < 2y_{yz}/y_0 - z_{yz}/z_0 < 1, \quad \text{and} \tag{29b}$$

Downloaded From: https://www.spiedigitallibrary.org/journals/Optical-Engineering on 10 Feb 2022
Terms of Use: https://www.spiedigitallibrary.org/terms-of-use

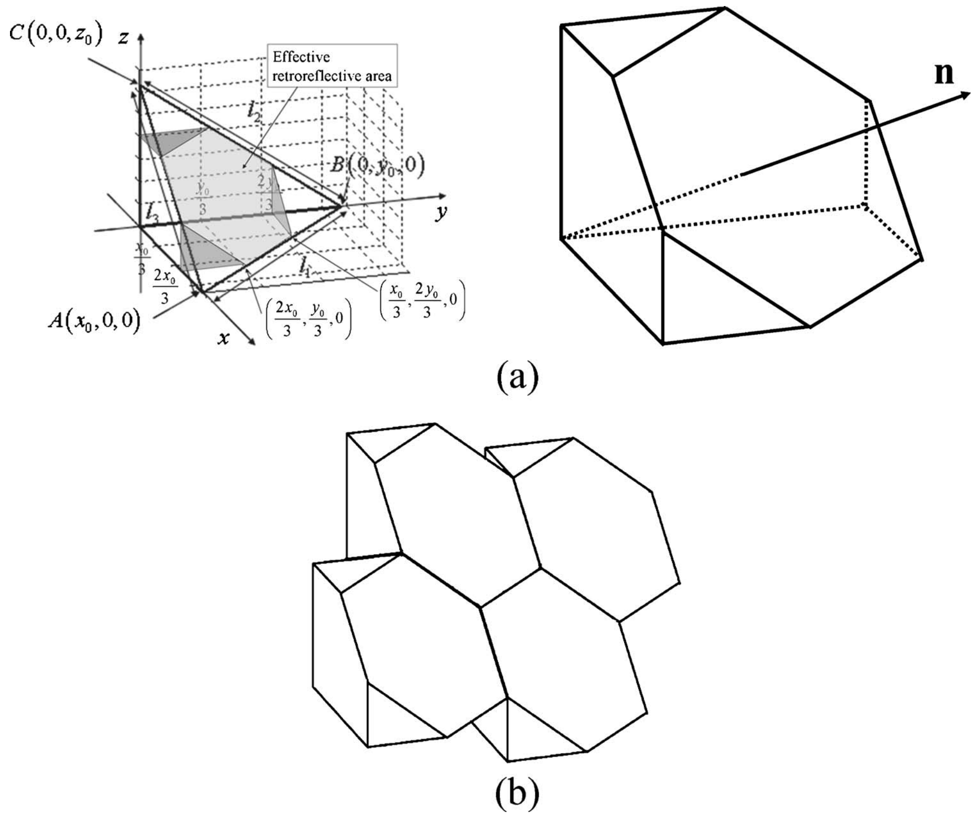

Fig. 10 (a) Polyhedron structure having the effective retroreflective area ratio of 100%. (b) Periodic arrangement of the corner-cubes with the effective retroreflective area ratio of 100%.

$$-1 < 2z_{yz}/z_0 - y_{yz}/y_0 < 1; \tag{29c}$$

and in the z-x plane, we obtain

$$-1 < z_{zx}/z_0 + x_{zx}/x_0 < 1, \tag{30a}$$

$$-1 < 2z_{zx}/z_0 - x_{zx}/x_0 < 1, \quad \text{and} \tag{30b}$$

$$-1 < 2x_{zx}/x_0 - z_{zx}/z_0 < 1. \tag{30c}$$

The regions in the x-y plane, the y-z plane, and the z-x plane are plotted in Figs. 9(a)–9(c). From the above analysis, we know that the area near the apex points of the corner-cube do not actually contribute the retroreflection. The effective volumetric region of the corner-cube through which rays pass can be sufficiently constrained by the polyhedron indicated in Fig. 10(a). Theoretically, this polyhedron structure has a 100% effective retroreflective area ratio while conventional sheets[2] have an effective retroreflective area ratio less than 67%. Fortunately, this shape is appropriate for the tight and periodic arrangement. Figure 10(b) illustrates the periodic arrangement of the corner-cubes with a 100% effective retroreflective area ratio.

In Fig. 11, some design examples of the corner-cubes for different incident optical ray bundles are presented for a comparison. They include the optimal corner-cube structures for the incident optical ray bundles with the incidence angle $\theta''=0$ deg and the azimuth angle $\phi''=0$ deg; the incidence angle $\theta''=30$ deg and the azimuth angle $\phi''=90$ deg; the incidence angle $\theta''=50$ deg and the azimuth angle $\phi''=90$ deg; and the incidence angle $\theta''=30$ deg; and the azimuth angle of $\phi''=270$ deg.

4 Conclusion

In conclusion, an optimal retroreflection corner-cube sheet structure with an effective retroreflective area ratio of 100% has been designed based on a geometric optics analysis. A mathematical theorem and a corollary about the optimal corner-cube structure were also derived, and the analytic design formulas of optimal corner-cube were obtained. A novel packing method was proposed of optimally designed elementary corner-cubes for constructing optimal retroreflection corner-cube sheets with the effective retroreflective area ratio of 100%. Since the retroreflection corner-cube sheet structure considered in this paper is the perfect retroreflector, the proposed structure is more promising for display applications such as head-mounted projective displays that require exact retroreflection than for conventional traffic safety applications, wherein intentional flaws in retroreflection are a key design factor.

Downloaded From: https://www.spiedigitallibrary.org/journals/Optical-Engineering on 10 Feb 2022
Terms of Use: https://www.spiedigitallibrary.org/terms-of-use

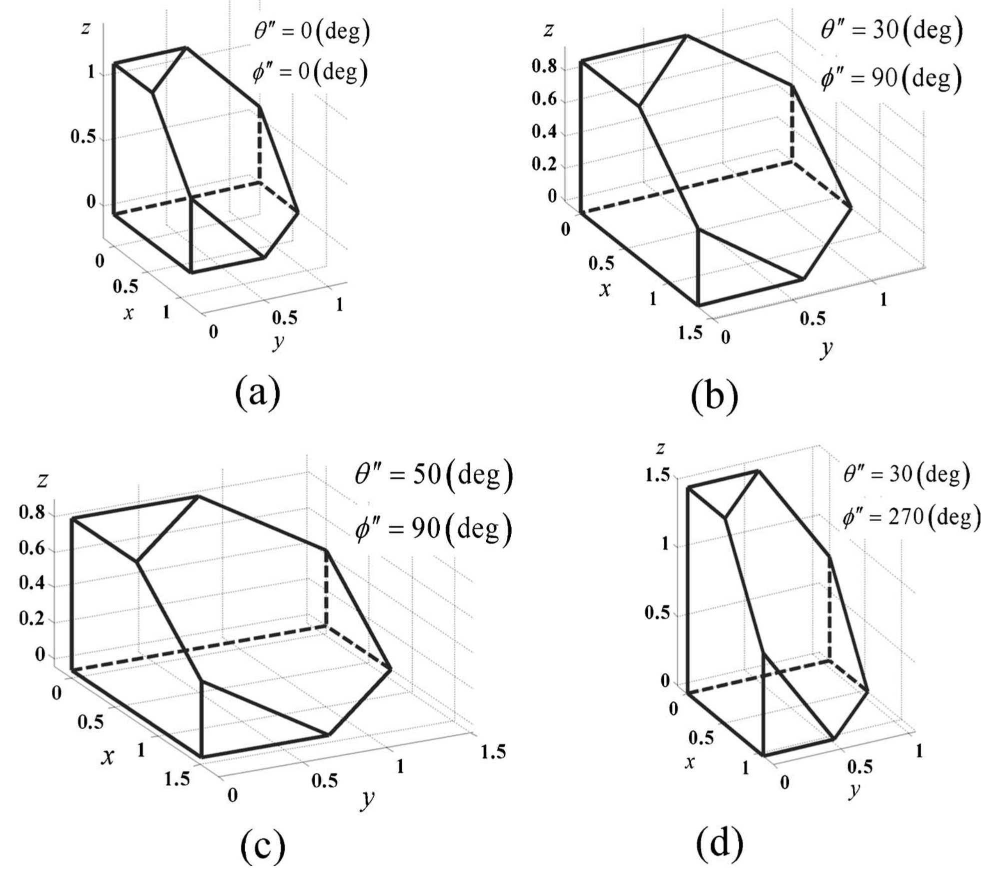

Fig. 11 Optimal corner-cube sheet structures for the incident optical ray bundles with (a) $\theta''=0$ deg, $\phi''=0$ deg; (b) $\theta''=30$ deg, $\phi''=90$ deg; (c) $\theta''=50$ deg, $\phi''=90$ deg; and (d) $\theta''=30$ deg, $\phi''=270$ deg.

References

1. Commission International de L'Eclairage, "Retroreflection: definition and measurement," Publication CIE 54.202001 (2001).
2. R. B. Nilsen and X. J. Lu, "Retroreflection technology," *Proc. SPIE* **5616**, 47–60 (2004).
3. D. C. O'Brien, G. E. Faulkner, and D. J. Edwards, "Optical properties of a retroreflecting sheet," *Appl. Opt.* **38**, 4137–4144 (1999).
4. G. H. Seward and P. S. Cort, "Measurement and characterization of angular reflectance for cube-corners and microspheres," *Opt. Eng.* **38**, 164–169 (1999).
5. S. E. Segre and V. Zanza, "Mueller calculus polarization change in the cube-corner retroreflector," *J. Opt. Soc. Am. A* **20**, 1804–1811 (2003).
6. W. H. Venable and N. L. Johnson, "Unified coordinate system for retroreflectance measurements," *Appl. Opt.* **19**, 1236–1241 (1980).
7. K. Hyyppa, "Signal response of a laser beam scanner," *Opt. Eng.* **33**, 2770–2776 (1994).
8. O. Nakamara, M. Goto, K. Toyoda, N. Takai, T. Kurosawa, and T. Nakamata, "A laser tracking robot-performance calibration system using ball-seated bearing mechanisms and a spherically shaped cat's eye retro-reflector," *Rev. Sci. Instrum.* **65**, 1006–1011 (1994).
9. B. E. Hines, "Optical truss and retroreflector modeling for picometer laser metrology," *Proc. SPIE* **1947**, 198–208 (1993).
10. R. A. Chipman, J. Shamir, H. J. Caulfield, and Q. Zhou, "Wave-front correcting properties of corner-cube arrays," *Appl. Opt.* **27**, 3203–3209 (1996).
11. K. S. J. Pister, D. S. Gunawan, and L. Lin, "Micromachined corner cube reflectors as a communication link," *Sens. Actuators, A* **46–47**, 580–583 (1995).
12. ASTM International, "Standard specification for retroreflective sheeting for traffic control," Publication ASTM D 4956-01 (2001).
13. 3M Corp., Product Catalog for Traffic Control Materials, 3M Traffic Control Materials Division, St. Paul, MN, http://www.3M.com/tcm (2003).
14. T. L. Hoopman, "Cube-corner retroreflective articles having wide angularity in multiple viewing planes," U.S. Patent 4,588,258 (1986).
15. R. Fisher, "Head-mounted projection display system featuring beam splitter and method of making same," U.S. Patent 5,572,229 (1996).
16. H. Hua, A. Girardot, C. Gao, and J. P. Rolland, "Engineering of head-mounted projective displays," *Appl. Opt.* **39**, 3814–3824 (2000).
17. J. Fergason, "Optical system for head mounted display using retro-reflector and method of displaying an image," U.S. Patent 5,621,572 (1997).
18. R. Kijima and T. Ojika, "Transition between virtual environment and workstation environment with projective head-mounted display," *Proc. IEEE VR 1997*, 130–137 (1997).
19. M. Inami, N. Kawakami, D. Sekiguchi, Y. Yanagida, T. Maeda, and S. Tachi, "Visuo-haptic display using head-mounted projector," *Proc. IEEE VR 2000*, 233–240 (2000).
20. H. Hua, C. Gao, F. Biocca, and J. P. Rolland, "An ultra-light and compact design and implementation of head-mounted projective displays," *Proc. of IEEE VR 2001*, 175–182 (2001).
21. H. Hua, L. Brown, and C. Gao, "SCAPE: supporting stereoscopic collaboration in augmented and projective environments," *IEEE Comput. Graphics Appl.* **24**, 66–75 (2004).
22. H. Kim and B. Lee, "Geometric optics analysis of light transmission and reflection characteristics of metallic prism sheets," *Opt. Eng.* **45**, 084004 (2006).

Hwi Kim received the B.S., M.S., and Ph.D. degrees in the School of Electrical Engineering from Seoul National University, Korea, in 2001 and 2003, and 2007, respectively. He is currently a post-doc researcher in the National Creative Research Center for Active Plasmonics Applications Systems, Seoul National University. His primary research interests are in the areas of plasmonics, nanophotonics, and transformation optics.

Downloaded From: https://www.spiedigitallibrary.org/journals/Optical-Engineering on 10 Feb 2022
Terms of Use: https://www.spiedigitallibrary.org/terms-of-use

Byoungho Lee received the B.S. and M.S. degrees in 1987 and 1989, respectively, from Seoul National University, Korea, in electronics engineering. He received a Ph.D. degree in 1993 from the University of California at Berkeley in electrical engineering and computer science. In 1994, he joined the faculty of the School of Electrical Engineering, Seoul National University, where he is now an associate professor. He became a Fellow of the SPIE in 2002 and a Fellow of the OSA in 2005. He is now serving as Director-at-large (Board of Directors) of OSA and a member of the Award Committee of Board of Directors of OSA. He is also serving as a member of the Engineering, Science and Technology Policy Committee of SPIE. He has served as a committee member for various international conferences. He has authored or coauthored more than 190 papers in international journals and more than 300 international conference papers. In 1999, his laboratory was honored as a National Research Laboratory by the Ministry of Science and Technology of Korea. In 2002 he received the Presidential Young Scientist Award of Korea. In 2007, his laboratory is honored as a National Creative Research Center for Active Plasmonics Applications Systems by the Ministry of Science and Technology of Korea. His research fields are hologram applications, three-dimensional displays, optical fiber gratings, plasmonics, and nanophotonics. Currently he is on the editorial boards of *Applied Optics*, *Optical Fiber Technology*, and *Journal of the Society for Information Display*.

Downloaded From: https://www.spiedigitallibrary.org/journals/Optical-Engineering on 10 Feb 2022
Terms of Use: https://www.spiedigitallibrary.org/terms-of-use